

# Multiple receptor states are required to describe both kinetic binding and activation of neutrophils via *N*-formyl peptide receptor ligands<sup>☆</sup>

Tamara L. Kinzer-Ursem<sup>a</sup>, Karyn L. Sutton<sup>a,b</sup>, Anna Waller<sup>a</sup>, Geneva M. Omann<sup>b,c,d</sup>, Jennifer J. Linderman<sup>a,\*</sup>

<sup>a</sup> Department of Chemical Engineering, University of Michigan, 3074 H.H. Dow Building, 2300 Hayward, Ann Arbor, MI 48109, USA

<sup>b</sup> Department of Surgery, University of Michigan, Ann Arbor, MI 48109, USA

<sup>c</sup> Department of Biological Chemistry, University of Michigan, Ann Arbor, MI 48109, USA

<sup>d</sup> VA Medical Center, Ann Arbor, MI 48109, USA

Received 6 January 2006; accepted 23 January 2006

## Abstract

It is well-established that the binding of *N*-formyl peptides to the *N*-formyl peptide receptor on neutrophils can be described by a kinetic scheme that involves two ligand-bound receptor states, both a low affinity ligand–receptor complex and a high affinity ligand–receptor complex, and that the rate constants describing ligand–receptor binding and receptor affinity state interconversion are ligand-specific. Here we examine whether differences due to these rate constants, i.e. differences in the numbers and lifetimes of particular receptor states, are correlated with neutrophil responses, namely actin polymerization and oxidant production. We find that an additional receptor state, one not discerned from kinetic binding assays, is required to account for these responses. This receptor state is interpreted as the number of low affinity bound receptors that are capable of activating G proteins; in other words, the accumulation of these active receptors correlates with the extent of both responses. Furthermore, this analysis allows for the quantification of a parameter that measures the relative strength of a ligand to bias the receptor into the active conformation. A model with this additional receptor state is sufficient to describe response data when two ligands (agonist/agonist or agonist/antagonist pairs) are added simultaneously, suggesting that cells respond to the accumulation of active receptors regardless of the identity of the ligand(s).

© 2006 Elsevier Inc. All rights reserved.

**Keywords:** Kinetic rate constants; Upregulation; Internalization; fMLP receptor; Agonism; Actin; Oxidant; Leukocyte; Potency; Mathematical model

## 1. Introduction

All agonists are not equal in terms of receptor pathway activation [1–3]. This has been explained in terms of selective stabilization of different active receptor states [4,5]. However it is

*Abbreviations:* GPCR, G protein coupled receptor; CHO-NLFFNYK-FL, *N*-formyl-norleucyl-leucyl-phenylalanyl-norleucyl-tyrosyl-lysine-fluorescein; CHO-NLFFNYK-TMR, *N*-formyl-norleucyl-leucyl-phenylalanyl-norleucyl-tyrosyl-lysine-tetramethylrhodamine; CHO-NLF, *N*-formyl-norleucyl-leucyl-phenylalanine; CHO-MLF, *N*-formyl-methionyl-leucyl-phenylalanine; CHO-MLFFK-FL, *N*-formyl-methionyl-leucyl-phenylalanyl-phenylalanyl-lysine-fluorescein; CHO-VLFFK-FL, *N*-formyl-valyl-leucyl-phenylalanyl-lysine-fluorescein; tBoc, *t*-Boc-Phe-D-Leu-Phe-D-Leu-Phe-OH.

<sup>☆</sup> This work was supported by the NIH GM62930 (J.J.L.) and the Office of Research and Development, Medical Research Service, Department of Veteran Affairs (GMO).

\* Corresponding author. Tel.: +1 734 763 0679; fax: +1 734 763 0459.

*E-mail address:* [linderman@umich.edu](mailto:linderman@umich.edu) (J.J. Linderman).

also possible that the kinetic lifetimes of particular ligand–receptor complexes play an important role in determining signaling outcomes [6,7]. In other words, different ligands may produce not only different numbers but also different lifetimes of receptor states relevant to production of particular responses. Here we use a combined experimental and modeling approach to investigate the role of dynamic ligand–receptor binding, receptor trafficking, and receptor state changes in determining response characteristics for a specific G protein coupled receptor (GPCR) system.

The *N*-formyl peptide receptor on human neutrophils<sup>1</sup> binds byproducts of bacterial protein synthesis (*N*-formyl peptides),

<sup>1</sup> We note that the *N*-formyl peptide receptor has been cloned and homologs have been identified by low-stringency cross-hybridization with a cDNA from this clone (reviewed in [52]). One of these homologs, FPRL-1, is present in neutrophils at very low expression levels and exhibits low affinity for *N*-formyl peptides [53,54]. We have previously confirmed that this homolog does not significantly contribute to our binding or response measurements [10].

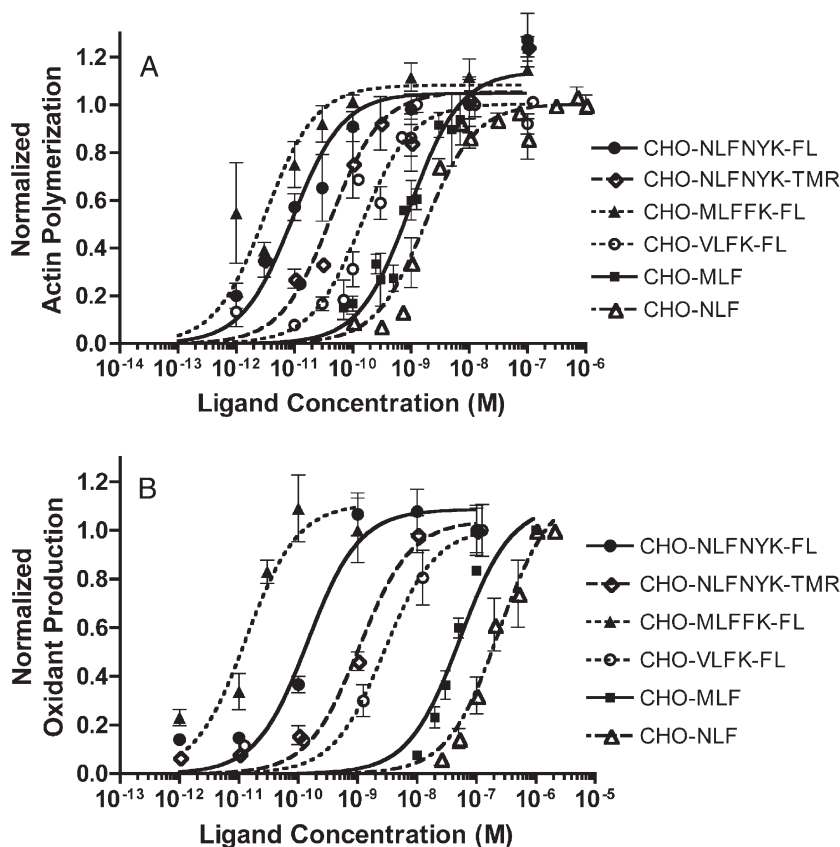


Fig. 1. Ligand potency varies over 3 to 4 orders of magnitude for six agonists for the *N*-formyl peptide receptor on human neutrophils. (A) Normalized magnitude of actin polymerization. Reported  $ED_{50}$  concentrations: CHO-MLFFK-FL  $3 \times 10^{-12}$ , CHO-NLFNYK-FL  $9 \times 10^{-12}$ , CHO-NLFNYK-TMR  $4 \times 10^{-11}$ , CHO-VLFK-FL  $1 \times 10^{-10}$ , CHO-MLF  $1 \times 10^{-9}$ , CHO-NLF  $2 \times 10^{-9}$  (M). (B) Normalized magnitude of oxidant production. Reported  $ED_{50}$  concentrations: CHO-MLFFK-FL  $2 \times 10^{-11}$ , CHO-NLFNYK-FL  $2 \times 10^{-10}$ , CHO-NLFNYK-TMR  $1 \times 10^{-9}$ , CHO-VLFK-FL  $4 \times 10^{-9}$ , CHO-MLF  $3 \times 10^{-8}$ , CHO-NLF  $2 \times 10^{-7}$  (M). Data taken from Waller et al. (2004) [10].

resulting in G protein activation and G protein dependent cellular responses including chemotaxis and oxidative burst [8,9]. Real-time spectrofluorometric measurements of actin polymerization (chemotaxis) and oxidant production (oxidative burst) have previously been reported for six *N*-formyl peptides and are presented for reference in Fig. 1 [10]. The time scales of these responses are very rapid (10–200s), occurring well before ligand-binding reaches equilibrium (tens of minutes) [10–12]. While the efficacies of these six peptides for actin polymerization and oxidant production were found to be the same, potencies were found to vary over three orders of magnitude ( $3 \times 10^{-12}$  to  $2 \times 10^{-9}$  M) for actin polymerization and four orders of magnitude ( $2 \times 10^{-11}$  to  $2 \times 10^{-7}$  M) for oxidant production [10].<sup>2</sup> Additionally, GTP $\gamma$ S binding studies on human neutrophil membranes gave dose response curves that are similar to those measured for actin polymerization and oxidant production. All six agonists tested were full agonists for GTP $\gamma$ S binding and the potency range spanned four orders of magnitude, implying that ligand potency and efficacy for actin

polymerization and oxidant production are determined at or before G protein activation [10].

A particular advantage to this system is that the dynamics of ligand–receptor binding have been carefully characterized at 4°C, a temperature at which receptor trafficking to and from the surface is negligible, using fluorescently labeled ligands and real-time, flow cytometric methods for a range of *N*-formyl peptides [10,11,13–18]. Significantly, the ligand–receptor binding and receptor affinity conversion rate constants are ligand-dependent, suggesting that ligand-specific differences in kinetics may contribute to differences in ligand potency and responses [10]. Previous work with the *N*-formyl peptide receptor points toward the temporal history of the low affinity bound receptor as a controlling factor when analyzing the dynamic responses of actin polymerization and oxidant production [9,19].

Relating the kinetics of ligand–receptor binding (including receptor affinity conversion) and receptor trafficking to cellular responses, however, requires values for binding and receptor trafficking parameters at physiological temperature. In this work we used two approaches to gather 37°C kinetic binding constants for *N*-formyl peptides of interest. First, we directly measured ligand–receptor binding and receptor trafficking of two fluorescein labeled *N*-formyl peptides (CHO-MLFFK-FL and CHO-VLFK-FL) and calculated the binding parameters

<sup>2</sup> We refer to the maximum ability of a ligand to induce a response at saturating concentrations as “efficacy”. “Potency” is quantified by a ligand’s  $ED_{50}$  concentration for a particular response.

using a well-characterized kinetic binding model. Second, we employed an approach of using 4°C binding parameters to estimate 37°C values. This was done for non-fluorescent ligands (CHO-MLF, CHO-NLF, and tBoc) and for one fluorescent ligand (CHO-NLFNYK-TMR), which exhibits fluorescence characteristics that are not optimal for this study.

With these data in hand we are in a unique position to determine whether the receptor-level events described by binding and trafficking models are sufficient to account for ligand-specific differences in cellular responses in this G protein coupled receptor system. We hypothesize that the ligand-specific differences in the dynamic lifetimes of the low affinity ligand–receptor complex may be a major determinant of downstream cellular responses, i.e. actin polymerization and oxidant production, in the *N*-formyl peptide receptor system on human neutrophils. Although one might build a detailed model incorporating the signal transduction network linking ligand–receptor complexes and response generation, many of the details of these pathways, and certainly many of the critical parameters (rate constants and concentrations), are unknown. We choose here a simpler approach, based on evidence described earlier [9–12,19] suggesting that the ligand-dependent characteristics of responses are determined by the dynamic events that occur at or near the level of the receptor.

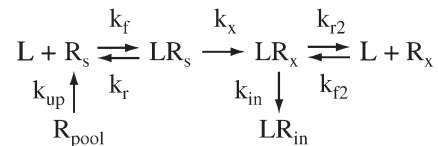
Using 37°C binding rate constants for seven *N*-formyl peptide receptor ligands we simulate dynamic ligand–receptor complex formation and correlate the time history of complex formation with response. We find that the observed binding kinetics alone do not account for differences in ligand potency and show that the addition of an ‘active’ receptor state is necessary. Importantly, incorporation of this additional receptor state allows for a relative measure of the ability of a ligand to bias the receptor into an active conformation. Using this quantitative approach we also find that this new model accounts for actin polymerization elicited by simultaneous stimulation with multiple ligands, suggesting that cells sum the contribution of active receptor complexes regardless of ligand identity.

## 2. Binding models

### 2.1. 37°C kinetic binding model

It is well established that the binding of ligands to the neutrophil *N*-formyl peptide receptor is described by an interconverting receptor binding scheme in which peptides bind to receptor with either low affinity or high affinity and ligand–receptor complexes in a low affinity state can irreversibly convert to a high affinity state [8,20,21]. The receptor-level events involved in binding of ligand and receptor trafficking at 37°C can be described in Scheme 1.

Ligand (*L*) binds to surface receptors ( $R_s$ ) with rate constant  $k_f$  to form low affinity ligand–receptor complexes ( $LR_s$ ), which convert irreversibly to high affinity complexes ( $LR_x$ ) with rate constant  $k_x$ . High affinity complexes are also formed by ligand binding to high affinity receptors ( $R_x$ ) with the rate constant  $k_{f2}$ . Ligand can dissociate from low or high affinity ligand–receptor complexes with rate constants  $k_r$  and  $k_{r2}$ , respectively. At 37°C,



Scheme 1. 37°C binding model.

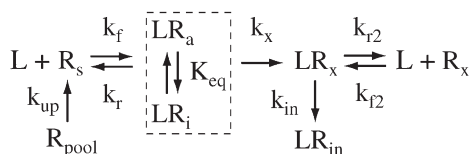
but not at 4°C, surface receptors ( $R_s$ ) are upregulated from an internal pool of receptors ( $R_{pool}$ ) with a rate constant of  $k_{up}$  and high affinity receptor complexes ( $LR_x$ ) are internalized ( $LR_{in}$ ) with a rate constant of  $k_{in}$ . The low affinity ligand–receptor complex is believed to be responsible for G protein activation, while the high affinity complex is generally thought to be a desensitized or phosphorylated state [9,22–24]. It should be noted that this model does not explicitly include receptor recycling and as such may only represent events occurring over relatively short time scales (<30 min). Hence, total receptor number ( $R_{tot}$ ), equal to the sum of the receptor states described above, remains constant over the time period of kinetic data collection.

This is the simplest model that describes ligand binding to the *N*-formyl peptide receptor on human neutrophils at physiological temperature. Importantly, the values of many of the rate constants are ligand-dependent [10,18,21]. Of note are the kinetic parameters  $k_f$ ,  $k_r$  and  $k_x$ , which govern the formation and lifetime of the low affinity ligand–receptor complex ( $LR_s$ ). Due to the ligand-dependent values of these kinetic parameters there are ligand-specific differences in the dynamics of ligand–receptor complex formation and loss which may be critical for determining cellular response characteristics.

### 2.2. 37°C modified kinetic binding model

A second model of ligand–receptor binding and trafficking, shown in Scheme 2, is developed in this work. In the 37°C modified binding model (Scheme 2), all of the events described in the 37°C binding model (Scheme 1) are included. Thus Scheme 2 accounts for ligand binding exactly as in Scheme 1. In addition, Scheme 2 includes two conformations of the low affinity bound receptor state in order to incorporate the idea that GPCRs may exist in a number of conformational states with different abilities to signal. In support of this concept are theoretical equilibrium models such as the extended and cubic ternary complex models in which GPCRs exist in multiple conformational states, some of which may be able to elicit responses [25–28], recent experimental data from the well-studied  $\beta_2$ -adrenergic system suggesting that ligands induce distinct micro-conformations in the  $\beta_2$ -adrenergic receptor [29–31], and studies of mutant *N*-formyl peptide receptors that demonstrate that *N*-formyl peptide receptors also take on multiple conformations [14,32,33]. Here we represent this concept by introducing two low affinity receptor states, one that can activate second messengers ( $LR_a$ ) and one that does not significantly participate in signal transduction ( $LR_i$ ). An alternative way to represent this concept is presented in the discussion.

Scheme 2 is the simplest model that can be proposed to incorporate multiple states of the low affinity bound receptor.



Scheme 2. 37°C modified binding model.

Ligand (L) binds to surface receptors ( $R_s$ ) to form one of two low affinity ligand–receptor complexes ( $LR_a$  or  $LR_i$ ). Ligand is assumed to bind and dissociate from both receptor states similarly, with rate constants  $k_f$  and  $k_r$  respectively. Note that there may in fact be differences in the association and dissociation kinetic constants for the different states, but that these differences are not detectable in our system with currently available techniques.  $LR_a$  is assumed to be the active form of the complex and is able to activate G protein; all  $LR_a$  are assumed to have an equal ability to activate G protein.  $LR_i$  is assumed to be an inefficient signaling complex and therefore does not significantly contribute to initiation of cellular response. These complexes are assumed to exist in rapid equilibrium and the ratio  $LR_a/LR_i$  is defined as the equilibrium constant  $K_{eq}$ .  $K_{eq}$  is a ligand-dependent parameter that reflects the ability of the ligand to hold the receptor in the active (signaling) conformation. In order to remain consistent with measured binding (Section 3.3), the sum of the two low affinity bound receptor states in Scheme 2 is equal to the number of low affinity bound receptor states in Scheme 1 ( $LR_s = LR_a + LR_i$ ). Equations describing both models can be found in Appendix B.

### 3. Experimental methods

#### 3.1. Reagents

Standard cellular and ligand buffer, HSB, contained 5 mM KCl, 147 mM NaCl, 1.9 mM  $KH_2PO_4$ , 0.22 mM  $Na_2HPO_4$ , 5.5 mM glucose, 0.3 mM  $MgSO_4$ , 1 mM  $MgCl_2$ , and 10 mM HEPES, at pH 7.4. To decrease loss of peptide ligand to non-specific binding during ligand dilutions, 1 mg/ml (0.1%) bovine serum albumin (BSA) was added to HSB. BSA, CHO-MLF, CHO-NLF, and fluorescein were obtained from Sigma Chemical Co. (St. Louis, MO). CHO-NLFNYK-FL and CHO-NLFNYK-TMR were obtained from Molecular Probes, Inc (Eugene, OR). CHO-MLFFK-FL and CHO-VLFFK-FL were synthesized, purified, and characterized as previously described [10,13]. tBoc was purchased from Bachem Biosciences Inc. (King of Prussia, PA). All other reagents were purchased from Sigma Chemical Company (St. Louis, MO) and were of analytical grade.

#### 3.2. Neutrophil isolation

Neutrophils were isolated from healthy donor blood by density gradient centrifugation on neutrophil isolation medium 1-Step Polymorphs (Accurate Chemical and Scientific Corp, Westbury, NY). Briefly, 30 ml aliquots of healthy donor blood were mixed with 350  $\mu$ l 0.5 M EDTA. 10 ml aliquots of this

mixture were then layered on top of 7 ml isolation medium and centrifuged at 1600 rpm for 60 min at 24°C. The neutrophil layer was then collected and washed in HSB with 1.5 mM  $Ca^{2+}$  at 4°C. The red blood cells were removed using hypotonic lysis by resuspending the pellet with 4.5 ml  $H_2O$  and then rapidly restoring isotonicity by adding 0.5 ml 9% saline solution. Saline solution and cellular debris from lysis were discarded after centrifugation at 1600 rpm for 10 min at 4°C. Cells were then washed in HSB, counted on a hemocytometer, and brought to a concentration of  $1 \times 10^8$  cells/ml. Cells were stored at 4°C in HSB prior to use.

#### 3.3. Measurement of ligand–receptor binding and trafficking kinetics at 37°C

The kinetics of ligand–receptor binding at 37°C for CHO-MLFFK-FL and CHO-VLFFK-FL were measured as previously described [10,21]. Briefly, neutrophils at  $10^6$ /ml in HSB plus  $Ca^{2+}$  (1.5 mM  $CaCl_2$ ) were warmed for 10 min and then placed on a flow cytometer (Lysis II software, FACScan, Becton Dickinson). After 10 s of baseline measurement the sample was taken from the instrument and ligand was added with data collection resuming less than 4 s after addition of ligand. Non-specific binding was determined in the presence of excess CHO-MLF. Association and dissociation protocols were used to monitor the kinetic binding of CHO-MLFFK-FL and CHO-VLFFK-FL as previously described [13,16,21]. Dissociation was initiated at different time scales, after short times (15 to 90 s of binding) or after long times (more than 2 h of binding), in order to capture the different receptor affinity states. Measurement of receptor upregulation and internalization is described in Appendix A. Kinetic binding data were fit using MicroMath Scientist software (MicroMath Scientific Software, Salt Lake City, UT) to obtain estimates for  $k_f$ ,  $k_r$ ,  $k_x$ ,  $k_{r2}$ , and  $k_{r2}$ , while holding  $k_{up}$  constant for a given concentration at a value determined as described in Appendix A. Using these estimates, MicroMath Scientist software (MicroMath Scientific Software, Salt Lake City, UT) was used to extract  $k_{in}$  from the internalization data outlined in Appendix A. Iterations between binding and internalization data were used to determine the values for all seven parameters of Scheme 1.

#### 3.4. Estimation of ligand–receptor binding kinetics at 37°C using kinetics measured at 4°C

Measurement of ligand–receptor binding and trafficking kinetics at 37°C for non-fluorescent ligands (or ligands with fluorescence characteristics not optimal for the flow cytometer used) is complicated by the need to do competitive binding analysis [10,13,17]. The accompanying increase in the uncertainty of each parameter makes this time-consuming approach untenable. We chose instead another approach.

The effect of temperature on the rate of a chemical reaction is described by the Arrhenius equation

$$k = k_0 e^{(-E/RT)} \quad (1)$$

were  $k_0$  is a constant,  $E$  is the activation energy,  $R$  is the universal gas constant (1.987 cal/mol K), and  $T$  is temperature in Kelvin [18,21]. Previously published 4°C rate constants for all the ligands used in this study [10,13] were converted to 37°C estimates using Eq. (1) and an activation energy of 8000 cal/mol [18].

### 3.5. Actin polymerization assay

Dynamic actin polymerization was monitored by right angle light scattering on a spectrofluorometer (SLM-Aminco 8100, Urbana, IL) as described [9,34]. Briefly, cell solutions of  $1.5\text{--}2 \times 10^6$  cells/ml HSB plus 1.5 mM  $\text{Ca}^{2+}$  were incubated at 37°C for 10 min prior to assay. A baseline of cellular right angle light scatter at 340 nm was collected in a continuously stirred cuvette for the initial 20 s, at which time a bolus of ligand or ligand combinations was added (1/100 of the total sample volume) and the response monitored for an additional 60 s. Because of day-to-day variability in the maximum magnitude of change (likely due to donor variability), data from a particular day were normalized to the maximum magnitude of response of a saturating dose of CHO-NLFNYK-FL on that day. The concentrations of ligands that gave 50% maximal responses ( $\text{ED}_{50}$ ) were determined from fits of the data to a sigmoidal function using Prism version 4.0 for Macintosh (GraphPad Software, San Diego, CA).

## 4. Mathematical methods

### 4.1. Testing for relationships between signaling complexes and responses

We evaluated whether ligand-specific differences in responses of Fig. 1 could be explained by differences in  $\text{LR}_s$ , as determined by the ligand-specific differences in the rate constants of Scheme 1 or by differences in  $\text{LR}_a$ , as calculated via Scheme 2 and including equilibrium constant  $K_{\text{eq}}$ . Ligand–receptor binding and receptor trafficking events of Scheme 1 and 2 were simulated at varying ligand concentrations according to the equations given in Appendix B using Mathematica (Wolfram Research Inc., Champaign, IL). The time history of the number of signaling complexes was found by calculating the integral of  $\text{LR}_s$  (Scheme 1) or  $\text{LR}_a$  (Scheme 2) over an initial period (10 s) of ligand binding. Measured responses were then plotted vs. the calculated integral of  $\text{LR}_s$  (Scheme 1) or  $\text{LR}_a$  (Scheme 2).

### 4.2. Statistical analysis

Sigmoidal curve fits of the data were generated in Prism version 4.0 for Macintosh (GraphPad Software, San Diego, CA). Best-fit parameters from this nonlinear regression are given as mean  $\pm$  the standard error and were compared with one way ANOVA (analysis of variance) using InStat version 2.0.1 for Macintosh (GraphPad Software) to determine the statistical significance of the spread of the curves. Differences were considered statistically significant at  $p$ -values less than 0.05.

### 4.3. Accounting for uncertainty in rate constants

To account for uncertainty in values of the rate constants, predictions of the formation of the low affinity bound complex were also made for two limiting cases: high  $\text{LR}_s$  and low  $\text{LR}_s$  (Scheme 1) or high  $\text{LR}_a$  and low  $\text{LR}_a$  (Scheme 2). The rate constants that govern the magnitude of the signaling complex are  $k_f$ ,  $k_r$ , and  $k_x$ . Therefore, the prediction for the high case was made with a large value for  $k_f$  (original estimate plus reported standard error of the mean at 37°C) together with small values for  $k_r$  and  $k_x$  (original estimate minus reported standard error of the mean at 37°C). Conversely, the simulation for the low case was made with large values of  $k_r$  and  $k_x$  (original estimate plus standard error of the mean) and a small value for  $k_f$  (original estimate minus reported standard error of the mean). These high and low complex scenarios were included in the evaluation of  $K_{\text{eq}}$ .

### 4.4. Fitting $K_{\text{eq}}$ for the 37°C modified binding model

Although the kinetic rate constants were the same for both Schemes 1 and 2, the value of  $K_{\text{eq}}$  was unique to Scheme 2 and was calculated from the response data. It was assumed that the most potent ligand (CHO-MLFFK-FL) was most capable of biasing the receptor into a conformation that allowed for signaling ( $\text{LR}_a$ ). Thus  $K_{\text{eq}}$  was fixed for this ligand at a value of 1 and  $K_{\text{eq}}$  values for all other ligands were then determined by varying  $K_{\text{eq}}$  and simulating  $\text{LR}_a$  formation at the ligand's actin polymerization  $\text{ED}_{50}$  concentration so that the number of  $\text{LR}_a$  complexes was not significantly different from that of CHO-MLFFK-FL using an ANOVA test ( $p$ -value > 0.999 for the number of  $\text{LR}_a$  per cell at 10 s). This analysis allowed for a relative measure of the ability of a ligand to bias the receptor into an active conformational state. It was assumed that antagonists do not hold the receptor in the active conformation; therefore for an antagonist  $K_{\text{eq}}=0$ .

## 5. Results

### 5.1. Ligand–receptor binding kinetics at 37°C are evaluated for seven N-formyl peptide ligands

The kinetics of ligand–receptor association at 37°C for CHO-VLFFK-FL and CHO-MLFFK-FL are shown in Fig. 2. The kinetic binding constants obtained from association and dissociation protocols as described in Experimental methods and data fitting to Scheme 1 are listed in Table 1 along with those previously reported for CHO-NLFNYK-FL [21]. As an alternative to direct measurement at 37°C, kinetic rate constants for CHO-NLFNYK-FL, CHO-MLFFK-FL, and CHO-VLFFK-FL were calculated from their reported 4°C values [10,16,21] using Eq. (1) and these values are also listed in Table 1.

Most of the values of the calculated 37°C reaction rate constants are within two-fold of the measured rate constants at 37°C, with the exception of the calculated value for  $k_x$  of CHO-VLFFK-FL (20-fold difference). These small differences

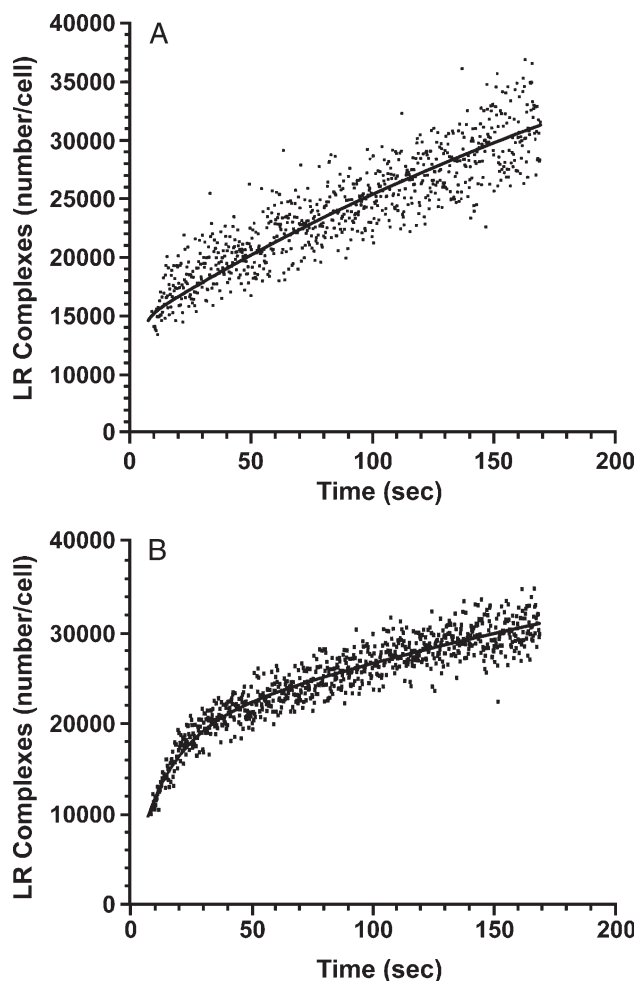


Fig. 2. A representative plot of the association of fluorescently labeled ligands at 37°C. Kinetic binding data (dots) and model fits (lines) are shown for ligand binding to the *N*-formyl peptide receptor collected via the association protocol described in Experimental methods. Both association and dissociation protocols were used to determine the 37°C kinetic rate constants of CHO-VLFK-FL and CHO-MLFFK-FL. (A) 10 nM CHO-VLFK-FL and (B) 1 nM CHO-MLFFK-FL.

in the values of the kinetic rate constants obtained by the two methods (consistent with previous reports [18,21]) did not impact the results of our analysis (Appendix A). Thus the

approximations of rate constants at 37°C based on previously reported 4°C rate constant values were employed for four of the ligands in this study (CHO-NLFNYK-TMR, CHO-MLF, CHO-NLF, tBoc) and are listed in Table 2. Measured values at 37°C were used for the other three ligands (CHO-NLFNYK-FL, CHO-MLFFK-FL, and CHO-VLFK-FL) and are also listed in Table 2.

### 5.2. Ligand–receptor binding and receptor trafficking kinetics alone cannot account for ligand-specific differences in cellular responses

The dynamic nature of LR<sub>s</sub> formation and loss is displayed in Fig. 3. For example, simulations of binding of 1 nM CHO-MLFFK-FL results in LR<sub>s</sub> formation that peaks at ~13 s with ~7500 LR<sub>s</sub> per cell. This maximum in LR<sub>s</sub> formation is followed by a rapid decline in the number of LR<sub>s</sub> per cell as LR<sub>s</sub> are converted to LR<sub>x</sub>. For comparison, binding of 1 nM CHO-NLF produces a slow increase in the number of LR<sub>s</sub> over the time course of cellular responses, approaching 250 LR<sub>s</sub> per cell at 300 s. These differences in LR<sub>s</sub> are a direct result of the measured differences in the ligand-dependent rate constants listed in Table 2.

The 37°C rate constants of Scheme 1 (Table 2) were used to calculate the accumulation of the low affinity ligand–receptor complex (LR<sub>s</sub>) over the initial 10 s of ligand binding (i.e. integrated LR<sub>s</sub>, or  $\int_0^{10} \text{LR}_s dt$ ). Integrated LR<sub>s</sub> values calculated for several ligand concentrations were then plotted against the corresponding response as shown in Fig. 4. If differences in ligand potency are accounted for by differences in the kinetics of ligand binding and receptor trafficking as they control the formation of signaling complexes (Scheme 1), the resulting plots of the calculated integrated numbers of signaling complexes (LR<sub>s</sub>) versus measured responses for each ligand will overlap. However, the values of integrated LR<sub>s</sub> that correspond to half maximal normalized actin polymerization range from 170 (s cell<sup>-1</sup>) for CHO-NLFNYK-TMR to 6000 (s cell<sup>-1</sup>) for CHO-NLF, and these differences are statistically significant ( $p$ -value=0.002) (Fig. 4A). Likewise, values of integrated LR<sub>s</sub> that correspond to half maximal normalized oxidant

Table 1  
Comparison of 37°C measured and 37°C estimated kinetic rate constants

Parameter	Rate constants <sup>a</sup>					
	CHO-NLFNYK-FL		CHO-MLFFK-FL		CHO-VLFK-FL	
	Arrhenius <sup>b,c</sup>	Measured <sup>c</sup>	Arrhenius <sup>b,d</sup>	Measured <sup>c</sup>	Arrhenius <sup>b,d</sup>	Measured <sup>c</sup>
$k_f$ ( $\times 10^7 \text{M}^{-1} \text{s}^{-1}$ )	3.5±0.2	8.4±2.0 (7)	4.0±0.4	12±0.2 (3)	1.9±0.5	1.1±0.4 (4)
$k_r$ ( $\times 10^{-1} \text{s}^{-1}$ )	5.2±0.3	3.7±1.0 (7)	2.3±0.2	1.7±0.2 (3)	3.5±0.9	2.7 (1)
$k_x$ ( $\times 10^{-2} \text{s}^{-1}$ )	11±0.5	6.5±1.0 (7)	7.5±0.5	4.9±0.3 (3)	0.08±0.03	1.2±0.09 (4)
$k_{r2}$ ( $\times 10^{-3} \text{s}^{-1}$ )	4.4±0.5	4.6±0.7 (3)	3.0±0.4	5.0±0.8 (3)	6.7±2.2	9.9±0.3 (2)
$k_{r2}$ ( $\times 10^6 \text{M}^{-1} \text{s}^{-1}$ )	9.4±0.9	84±20 (7)	69±0.9	80±4 (3)	10±5	ND <sup>f</sup>

<sup>a</sup> Values are given as the mean±standard error of mean of (*n*) measurements.

<sup>b</sup> Values determined at 4 °C were converted to 37 °C estimates using Eq. (1).

<sup>c</sup> Reported in Hoffman et al. [21].

<sup>d</sup> 4°C values reported in Waller et al. [10].

<sup>e</sup> Measured in this work.

<sup>f</sup> Not determined.

Table 2  
Agonist and antagonist kinetic binding constants at 37°C for Scheme 1 and 2

Parameter	Rate constants <sup>a</sup>						
	CHO-MLFFK-FL <sup>b</sup>	CHO-NLFNYK-FL <sup>c</sup>	CHO-NLFNYK-TMR <sup>d,e</sup>	CHO-VLFFK-FL <sup>b</sup>	CHO-MLF <sup>d,f</sup>	CHO-NLF <sup>d,f</sup>	tBOC <sup>d,f</sup>
$k_f$ ( $\times 10^7 M^{-1} s^{-1}$ )	12±0.2 (3)	8.4±2.0 (7)	1.4±0.09	1.1±0.4 (4)	5.4±1.8	18±7	0.39±0.04
$k_r$ ( $\times 10^{-1} s^{-1}$ )	1.7±0.2 (3)	3.7±1.0 (7)	5.4±0.2	2.7 (1)	25±6	110±30	80±19
$k_x$ ( $\times 10^{-2} s^{-1}$ )	4.9±0.3 (3)	6.5±1.0 (7)	6.7±0.4	1.2±0.09 (4)	0.049±0.005	0.045±0.02	0.18±0.1
$k_{r2}$ ( $\times 10^{-3} s^{-1}$ )	5.0±0.8 (3)	4.6±0.7 (3)	5.8±0.4	9.9±0.3 (2)	0.072±0.013	0.058±0.013	1.8±0.1
$k_{f2}$ ( $\times 10^6 M^{-1} s^{-1}$ )	80±4 (3)	84±20 (7)	2.8±0.2	10±5.0 <sup>d,e</sup>	0.0021	0.0002	0.001
$k_{up}$ ( $\times 10^{-10} s^{-1}$ )	12.5 <sup>g</sup>	4.5 <sup>g</sup>	1.3 <sup>g</sup>	0.4 <sup>g</sup>	0.08 <sup>g</sup>	0.02 <sup>g</sup>	0
$k_{in}$ ( $\times 10^{-3} s^{-1}$ )		3.3 <sup>h</sup>	3.3	1.2±0.07 (2)	3.3 <sup>h</sup>	3.3 <sup>h</sup>	3.3 <sup>h</sup>
	8.8±0.2 (3)						
$K_{ds}$ ( $\times 10^{-9} M$ )	1.4	4.4	39	25	46	61	2050
$K_{dx}$ ( $\times 10^{-9} M$ )	0.06	0.055	2.1	0.99	34	290	1500

<sup>a</sup> Values are given as the mean±standard error of mean of (*n*) measurements, or are estimated from parameter values at 4°C.

<sup>b</sup> Measured at 37°C.

<sup>c</sup> Reported in Hoffman et al. [21].

<sup>d</sup> Estimated from 4°C data using Eq. (1).

<sup>e</sup> 4 °C binding data reported in Waller et al. [13].

<sup>f</sup> 4 °C binding constants reported in Hoffman et al. [16].

<sup>g</sup> Values of  $k_{up}$  are ligand-specific and ligand-concentration-dependent.  $k_{up}$  values shown here are calculated at 1 nM ligand concentration (Appendix A).

<sup>h</sup> As reported in [21,22,51].

production range from 1000 ( $s\ cell^{-1}$ ) for CHO-MLFFK-FL to 130,000 ( $s\ cell^{-1}$ ) for CHO-NLF, and are also significantly different ( $p$ -value<0.001) (Fig. 4B). Qualitatively similar results are obtained by plotting normalized actin polymerization or normalized oxidant production as a function of initial rates of formation of LR<sub>s</sub> or as a function of the instantaneous value of LR<sub>s</sub> at 10s (actin polymerization) or 200s (oxidant production) (data not shown). Additionally, qualitatively similar results are obtained when plotting the rate of actin polymerization and rate of oxidant production as function of integrated LR<sub>s</sub>, instantaneous value of LR<sub>s</sub> at 10s or the initial rate of formation of LR<sub>s</sub> (data not shown). The range in values of integrated LR<sub>s</sub> that correspond to half maximal response generation was not significantly reduced from the range in values of ED<sub>50</sub> concentration from reported dose response curves [10] and listed in Fig. 1.

As a further test of the ability of Scheme 1 to account for ligand-induced differences in response generation we simulated

the formation of the high affinity form of the ligand–receptor complex, LR<sub>x</sub>. Fig. 5 shows time course of LR<sub>x</sub> formation at the actin polymerization ED<sub>50</sub> concentrations for each agonist. For the least potent ligand, CHO-NLF, simulations predict no more than 3LR<sub>x</sub> complexes per cell at the time of maximal actin polymerization (10s); it would seem unlikely that so few complexes would be capable of stimulating a maximal response. Additionally, CHO-NLFNYK-FL, a ligand with intermediate potency, generates the highest number of LR<sub>x</sub> complexes (18/cell) at the time of maximal actin polymerization. Thus, there is no correlation between the rank order of LR<sub>x</sub> complexes generated and rank order of ligand potency for actin polymerization. Similar results are found for oxidant production (data not shown). Therefore these responses cannot be reliably predicted from the production of LR<sub>x</sub>. Thus, while the 37°C binding model (Scheme 1) sufficiently describes ligand receptor binding and trafficking, it does not account for differences in ligand potency.

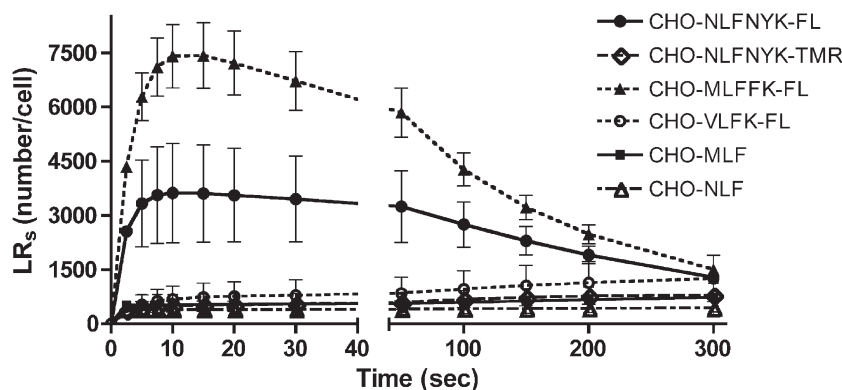


Fig. 3. Simulated formations and lifetimes of the low affinity ligand–receptor complex (LR<sub>s</sub> Scheme 1) vary for six agonists of the *N*-formyl peptide receptor at 1 nM and 37°C. Ligands with larger  $k_f$  values produce large number of LR<sub>s</sub> complexes rapidly. Ligands with larger  $k_x$  values show a rapid switch from LR<sub>s</sub> to LR<sub>x</sub> resulting in loss of LR<sub>s</sub>. Vertical error bars represent values for high and low simulations as described in Mathematical methods.

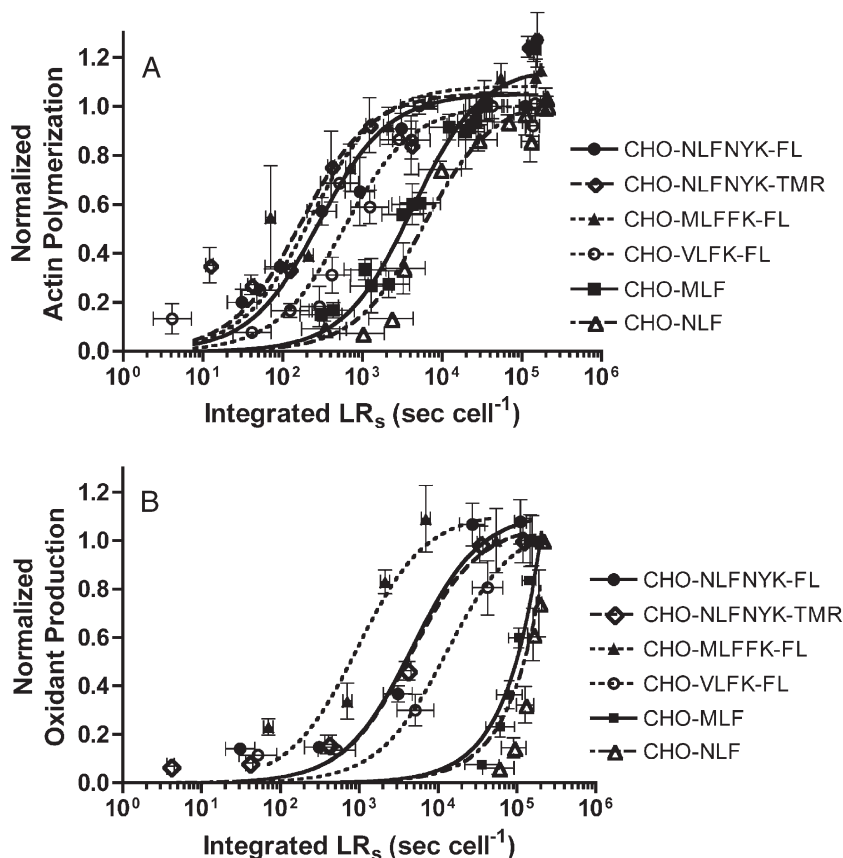


Fig. 4. Responses do not correlate with the temporal history of the low affinity LR<sub>s</sub> complex. (A) Normalized actin polymerization data are plotted as a function of the integrated number of LR<sub>s</sub> (Scheme 1) representing the accumulation of the low affinity ligand–receptor complex over the first 10s of ligand binding. (B) Normalized oxidant production data are plotted as a function of integrated number of LR<sub>s</sub> over the first 10s of ligand binding. Vertical error bars represent the error in the experimental measurements and horizontal error bars represent values for high and low simulations as described in Mathematical methods.

### 5.3. An additional receptor state allows for a quantitative relationship between active ligand–receptor complex formation and cellular responses

The equilibrium constant  $K_{eq}$  is introduced in Scheme 2 to account for ligand-specific ability to bias the receptor into active and inactive receptor states. As an example, Fig. 6A shows the effect of varying  $K_{eq}$  on the formation of LR<sub>a</sub> for

1 nM CHO-NLFNYK-FL. As  $K_{eq}$  decreases, the number of LR<sub>a</sub> formed decreases. Varying  $K_{eq}$  only affects the fraction of low affinity ligand–receptor complexes that are assumed to be participating in response generation. The  $K_{eq}$  values for each ligand were calculated by constraining the number of LR<sub>a</sub> formed at 10s to be the same as those formed for CHO-MLFFK-FL (the most potent ligand with  $K_{eq}=1$ ) as described in Mathematical methods and are listed in Table 3. Fig. 6B

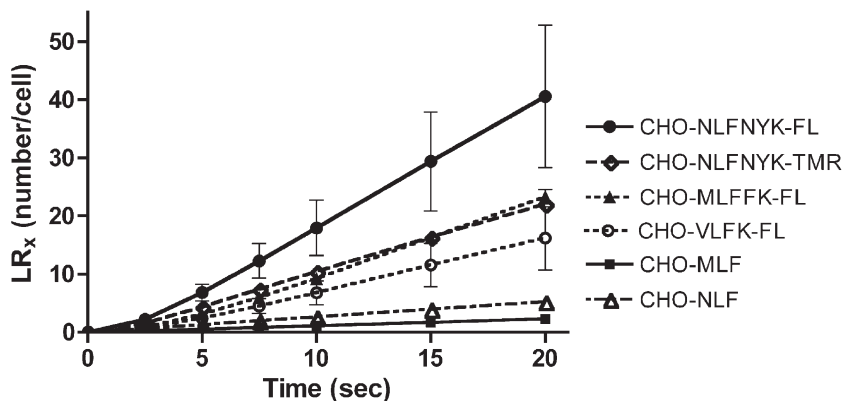


Fig. 5. Generation of LR<sub>x</sub> (Scheme 1) does not correlate with response generation. High affinity ligand–receptor complex (LR<sub>x</sub>) formation is simulated at 37°C and plotted over the first 20s of ligand binding at actin polymerization ED<sub>50</sub> concentrations (listed in Fig. 1). Vertical error bars represent values for high and low simulations as described in Mathematical methods.

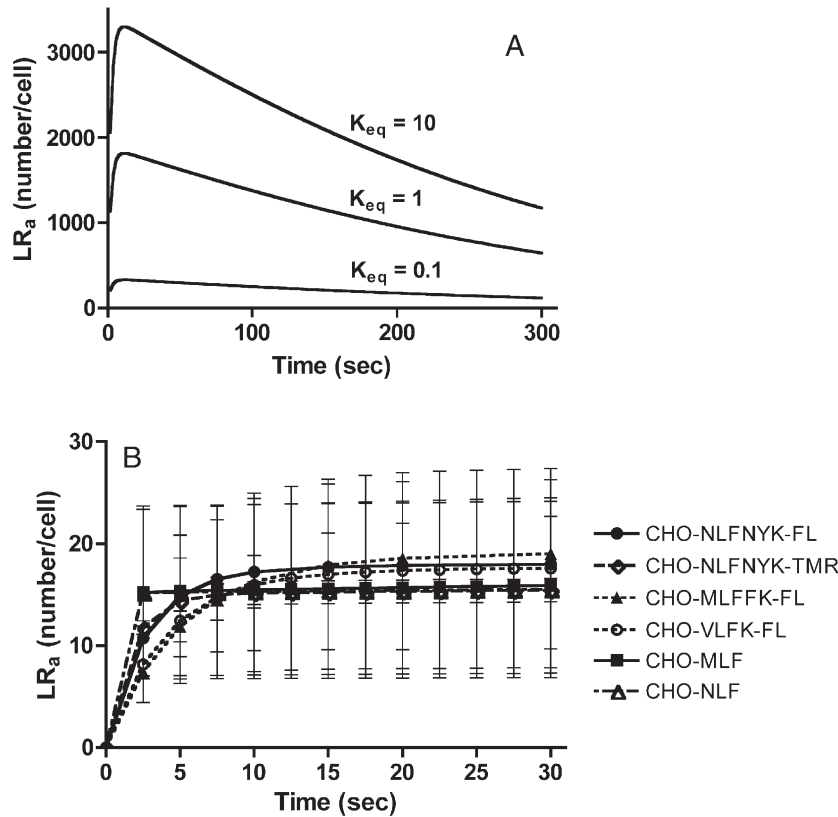


Fig. 6. Fitting  $K_{eq}$  to find the number of active low affinity signaling complexes ( $LR_a$ ) responsible for response generation. (A) The effect of varying  $K_{eq}$  on the number of active signaling complexes ( $LR_a$ ) for 1 nM CHO-NLFNYK-FL at 37°C. As  $K_{eq}$  decreases the number of active complexes decreases. (B) Finding  $K_{eq}$  for Scheme 2 for each ligand.  $K_{eq}$  was fit so that the numbers of active signaling complexes ( $LR_a$ ) are statistically similar as described in Mathematical methods. Ligand concentrations for simulation are equal to the  $ED_{50}$  concentration for actin polymerization. Vertical error bars represent values for high and low simulations, as described in Mathematical methods.  $K_{eq}$  values for each ligand are listed in Table 3.

shows simulations of  $LR_a$  formation for all six agonists at their respective actin polymerization  $ED_{50}$  concentrations and  $K_{eq}$  values.

Scheme 2 was solved for several ligand concentrations and the accumulation of active receptor complexes ( $LR_a$ ) over the initial 10s of ligand binding (i.e. integrated  $LR_a$ , or  $\int_0^{10} LR_a dt$ ) was calculated and plotted against the corresponding response as shown in Fig. 7. If differences in ligand potency are accounted for by differences in the kinetics of ligand binding and receptor trafficking together with differences in the ability of ligands to bias the receptor into an active state, the resulting plots of the calculated integrated  $LR_a$  versus measured responses for each ligand will overlap. Indeed plots of actin

polymerization versus integrated  $LR_a$  are not statistically different ( $p$ -value=0.9); the number of integrated  $LR_a$  required to produce a half maximal response (Fig. 7A) varies by less than 2-fold. This is a significant improvement over the 1000-fold difference in plots of normalized actin polymerization versus ligand concentration (compare to Fig. 1A). Qualitatively similar results are obtained by plotting normalized actin polymerization as a function of initial rates of formation of  $LR_a$ , or as a function of the instantaneous value of  $LR_a$  at 10s (data not shown). Actin polymerization is a rapid response and therefore it is expected that the correlation between the number of integrated active signaling complexes ( $LR_a$ ) over the initial 10s of ligand binding and response would be fairly strong. It should also be noted that the correlation of integrated  $LR_a$  and actin polymerization is in large part due to the use of actin polymerization  $ED_{50}$  concentrations in fitting  $K_{eq}$ .

Oxidant production has a longer time scale of response (approximately 200s) and therefore may not correlate as well to accumulation of  $LR_a$  over the initial 10s of ligand binding. However, plots of oxidant production versus the value of integrated  $LR_a$  over 10s of ligand binding for different ligands are not statistically different ( $p$ -value=0.8); the number of integrated  $LR_a$  required to produce a half maximal response varies only 10-fold (Fig. 7B) as compared to 10,000-fold for plots of normalized oxidant production versus ligand

Table 3  
Agonist and antagonist  $K_{eq}$  values for Scheme 2

Ligand	$K_{eq}$ value
CHO-MLFFK-FL	1
CHO-NLFNYK-FL	0.75
CHO-NLFNYK-TMR	3
CHO-VLFK-FL	0.3
CHO-MLF	0.03
CHO-NLF	0.02
tBoc	0

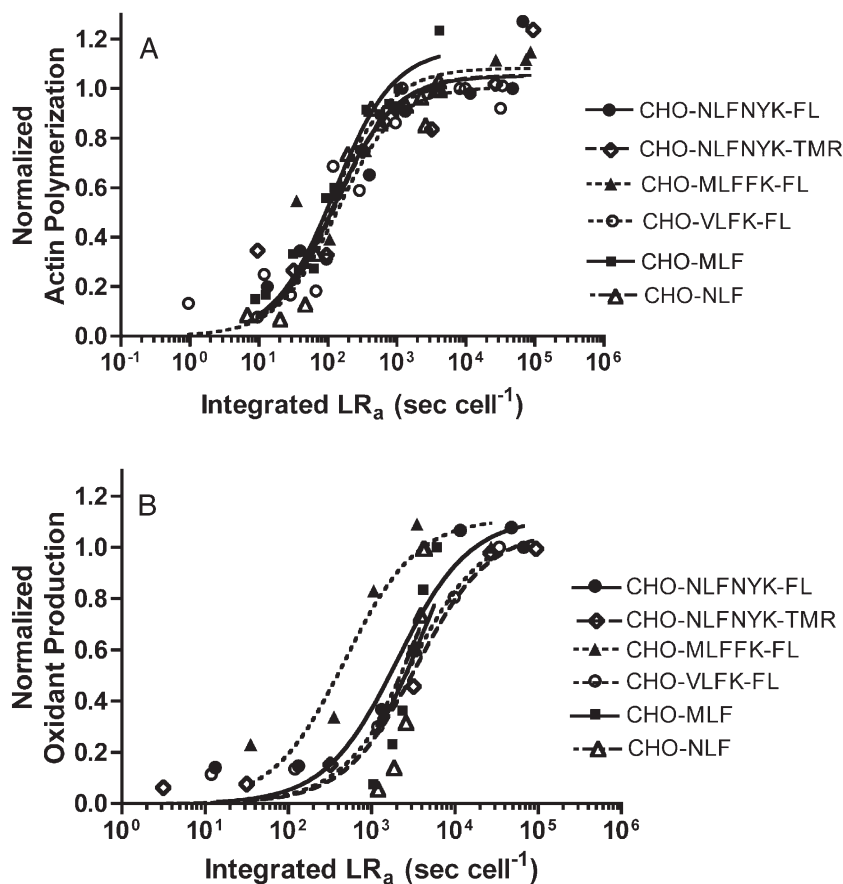


Fig. 7. Neutrophil responses are correlated to the temporal history of an active low affinity signaling complex ( $LR_a$ ). (A) Normalized actin polymerization data are plotted as a function of the integrated number of  $LR_a$  (Scheme 2) representing the accumulation of the active low affinity ligand–receptor complex over the first 10 s of ligand binding. (B) Normalized oxidant production data are plotted as a function of integrated number of  $LR_a$  over the first 10 s of ligand binding. Error bars have been omitted for clarity.

concentration (compare to Fig. 1B). Qualitatively similar results are obtained by plotting normalized oxidant production as a function of initial rates of formation of  $LR_a$  or as a function of the instantaneous value of  $LR_a$  at 10 s or 200 s (data not shown). Differences in ligand potency of 3 to 4 orders of magnitude in this system can therefore be explained by the accumulation of the active signaling complex  $LR_a$  over the initial seconds of ligand binding. Taken together, the alignment of curves in Fig. 7A and B also highlights the fact that the initial seconds of ligand binding are very important to these responses.

#### 5.4. The cellular response to multiple ligand stimulation correlates with active signaling complex ( $LR_a$ )

We next tested whether our model could be used to predict cellular responses when neutrophils were allowed to bind two ligands simultaneously. Actin polymerization was measured using right angle light scatter which decreases as actin polymerizes as described in Experimental methods. Combinations of agonist ligands were made to span the range of response generation, from expected low ( $1 \times 10^{-12}$  M CHO-NLFNYK-FL and  $1 \times 10^{-10}$  M CHO-MLF) to high ( $1 \times 10^{-10}$  M CHO-MLFFK-FL and  $1 \times 10^{-9}$  M CHO-VLFK-FL) stimulation. Several combinations of CHO-NLFNYK-FL and the antagonist

tBoc concentrations were also tested and are shown in Fig. 8A. As the antagonist concentration increases, it competes with CHO-NLFNYK-FL for binding, inhibiting the decrease in right angle light scatter.

Data in Fig. 7A were fit by a sigmoidal function to generate a predictive curve relating the accumulation of  $LR_a$  complexes with actin polymerization (Fig. 8B). If there is a correlation between multiple ligand-stimulated actin polymerization and the accumulation of  $LR_a$  then plots of integrated  $LR_a$  versus normalized actin polymerization will fall along the predictive curve. Merely summing the dose response curves for individual ligands would consistently over-estimate the actual response induced by simultaneous ligand addition because competition between ligands for receptor binding would not be taken into account. Equations allowing for competitive ligand binding (Appendix B) were solved for ligand concentrations corresponding to those of the ligand pairs used in the experimental measurements. Normalized actin polymerization induced by a range of concentrations of agonist–agonist and agonist–antagonist pairs is plotted as a function of integrated  $LR_a$  values in Fig. 8B. The measured responses fall along the curve as predicted with the largest deviation from the predictive curve (10-fold integrated  $LR_a$ ) occurring around half maximal response for the CHO-NLFNYK-FL and tBoc

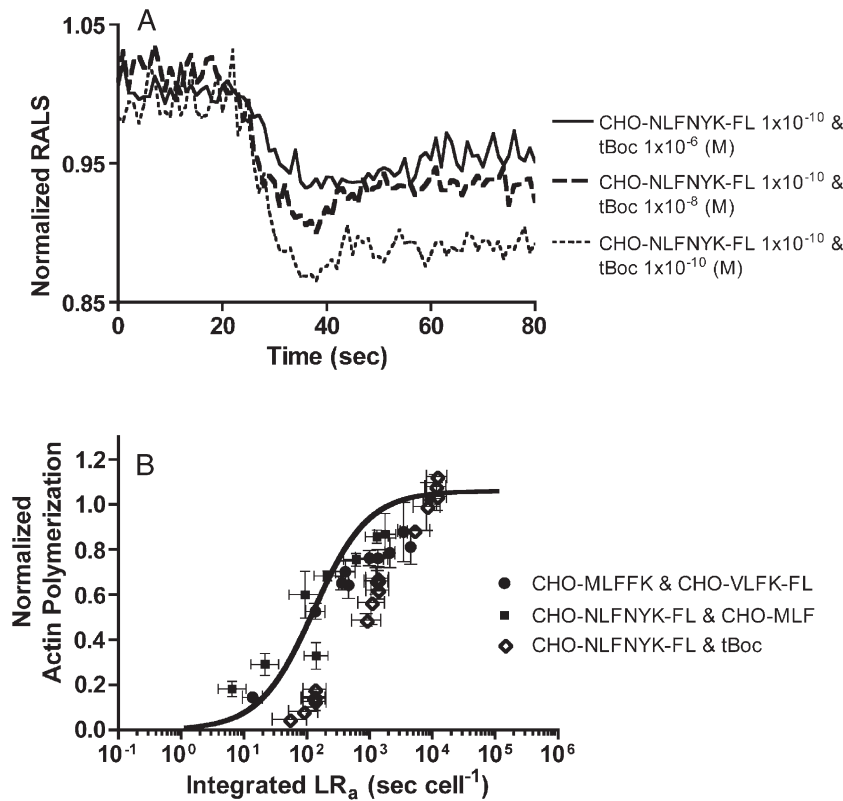


Fig. 8. Normalized actin polymerization induced by stimulating with two ligands simultaneously. (A) Normalized right angle light scatter measurements of neutrophil activation at varying concentrations of CHO-NLFNYK-FL and tBoc. (B) Normalized actin polymerization is plotted against values of integrated  $LR_a$  calculated at the respective ligand concentrations. The sigmoidal curve (solid line) is fit from the data of Fig. 6A and represents the correlation between single ligand stimulation and response. Vertical error bars represent the error in the experimental measurements and horizontal error bars represent values for high and low simulations as described in Mathematical methods.

paring.<sup>3</sup> These data are consistent with the concept of a cell that sums the activity from  $LR_a$  complexes regardless of ligand identity. Additionally, this result suggests that there are no cooperative interactions between ligands in receptor binding.

## 6. Discussion

Although signal transduction pathways are comprised of many molecules and reactions between the cell surface receptors and cellular responses, it is likely that ligand-specific differences are determined far upstream, at or near the receptor level, by interactions of the ligands themselves with receptors. The central goal of this work was to determine the relationship between the dynamics of these receptor-level events and cellular responses for a well-characterized system, the *N*-formyl peptide receptor on human neutrophils. To relate *N*-formyl peptide ligand binding and receptor trafficking to neutrophil responses at physiological temperature it was first necessary to obtain

values for rate constants at 37°C. 37°C binding and receptor trafficking rate constants were either measured or estimated from 4°C data. The values of these rate constants were ligand-specific, and the rate constant of receptor upregulation was also ligand concentration dependent (Appendix A).

The formation of low affinity ligand–receptor complexes ( $LR_s$ ) was simulated at physiological temperature using a well-established binding scheme with the addition of receptor upregulation and internalization (Scheme 1). Plots of the time history of  $LR_s$  over an initial period of ligand binding versus response generation (Fig. 5) were not able to explain differences in ligand potency. Similarly, response generation did not correlate with other measures of  $LR_s$  such as the number of complexes or the rate of formation of complexes. Several studies have reported that the high affinity form of the receptor ( $LR_x$ ) is a desensitized form of the receptor based on the long time scale of  $LR_x$  persistence and measurements of a high affinity surface receptor state that is associated with the cytoskeleton [9,35–37]. However, we have previously found that there may be a relationship between the formation of  $LR_x$  and response generation; in particular, we observed a correlation between the ligand-specific values of  $K_{dx}$  ( $k_{r2}/k_{f2}$ ) and response  $ED_{50}$  values [3]. Yet, by simulating the dynamic formation of  $LR_x$  at 37°C we found in this work that the formation of this high affinity form of the receptor did not correlate with differences in ligand potency for actin

<sup>3</sup> It should be noted that the measured responses of simultaneous agonist–agonist stimulation align with the predictive curve, while the agonist–antagonist (CHO-NLFNYK-FL - tBoc) response measurements lie slightly to the right of the predictive curve. This may be due to errors in estimating the 37 °C values of the kinetic rate constants of the antagonist or the assumption that tBoc does not produce any active low affinity signaling complexes ( $K_{eq}=0$  for antagonists). The latter would suggest that tBoc may produce  $LR_a$  but not enough to induce a detectable response.

polymerization or oxidant production. Taken together these results indicate that the measured ligand-specific differences in receptor binding and trafficking kinetics alone, i.e. numbers and lifetimes of receptors states in Scheme 1, cannot explain the differences in ligand potency.

Additional receptor states not included in Scheme 1 may be present but not detected in binding assays if the number of receptors in these additional states is small and/or if the binding kinetics are quite similar to those of other receptor states [38,39]. Using Scheme 2 we hypothesized that there exist at least two low affinity ligand–receptor complexes and that these active ( $LR_a$ ) and inactive ( $LR_i$ ) states can contribute to differences in ligand potency. As examples, CHO-NLFNYK-TMR and CHO-MLF are predicted to have  $\sim 75\%$  and  $\sim 3\%$  of their low affinity ligand–receptor complexes in the  $LR_a$  state, respectively (Table 3). That Scheme 1 fits the binding data for all ligands well, together with the observation that  $K_{ds}$  ( $=k_r/k_f$ ) is similar for all 7 ligands (Table 2, and [10,16]), suggests very similar binding characteristics for both states  $LR_a$  and  $LR_i$ .

Using Scheme 2 we find that the accumulation of an active receptor state ( $LR_a$ ) over the initial 10s of ligand binding is sufficient to describe activation of both actin polymerization and oxidant production via the *N*-formyl peptide receptor. Although the ligand binding kinetics of Scheme 1 alone are not sufficient to describe the responses, information from Scheme 1 was vital to informing the choice of Scheme 2 and guiding the focus to early receptor states. These rapid receptor activation events ( $\sim 10$ s) determine responses at longer times, such as oxidant production ( $\sim 200$ s). In other words, both the lifetime and the ratio of active to inactive low affinity ligand–receptor complexes contribute to the character of signaling in the system.

The ligands investigated here are either full agonists (Fig. 1) or antagonists. *N*-formyl peptide-induced actin polymerization is very sensitive to the number of ligand–receptor complexes generated upon ligand binding. Sklar and colleagues have reported that only 0.2% of the receptors are occupied ( $LR_s + LR_x$ ) at the time of maximal actin polymerization (10s) with 0.01 nM CHO-NLFNYK-FL [11]. Our model predicts that at this time and concentration approximately 20 active complexes ( $LR_a$ ) would be sufficient for maximal actin polymerization. Given this sensitivity, it has been notoriously difficult to find partial agonists for the *N*-formyl peptide receptor on human neutrophils, although there has been one report [40]. We note that in other GPCR systems Scheme 2 would be fully capable of accounting for partial agonism.

Scheme 2 introduces only one additional parameter into an already established kinetic binding model and suggests that a minimum of two low affinity ligand–receptor complexes are necessary to describe these responses, although more may exist [25,41]. The time history of  $LR_a$  complexes correlates well with responses without including intracellular signaling events that are known to be important for signal amplification in neutrophils [42–44]. Furthermore, we find that Scheme 2 can account for activation of neutrophils when stimulated simultaneously by multiple ligands to the *N*-formyl peptide receptor (Fig. 8). Thus Scheme 2 represents the simplest kinetic model that can be used to describe both ligand binding and response

generation in the *N*-formyl peptide receptor system. Alternatively, a model incorporating a spectrum of ligand-specific receptor conformations could be employed with the implication that each conformation would possess a slightly different ability to activate G protein. There would in essence be a ligand-specific activation rate constant for the interaction of  $LR_s$  with G protein. This additional ligand-specific parameter would function similarly to the ligand-specific parameter  $K_{eq}$  introduced in Scheme 2. Thus for our purposes these models would be equivalent.

This is the first study to quantify the relative strength of a ligand to bias receptor into an active conformation (Table 3) by focusing on *dynamic* ligand–receptor binding and receptor trafficking and their relationship to responses. In contrast, many previous models of GPCR activation that seek to correlate ligand–receptor binding to response generation are equilibrium models [27,28,45–47]. In these models (e.g. extended or cubic ternary complex models) the parameter  $\alpha$  has been used to describe the ability of a ligand to bias the receptor into an active conformation [27,28]. Here we use a similar parameter ( $K_{eq}$ ) in a kinetic model to quantify the relative ability of a ligand to bias the receptor into an active conformation state.

Finally, the work presented here highlights the need for kinetic studies to focus on rapid ligand–receptor binding events that occur prior to equilibrium binding. This is the first study to use a kinetic framework based on direct measurements of receptor binding, upregulation and internalization to relate the initial events in GPCR signaling to multiple cellular responses for a set of ligands. These types of studies, in concert with the significant amount of work being done in the area of receptor conformation [29–31,48,49], will provide a basis for fully elucidating the underlying mechanisms of GPCR signal transduction and allow for prediction and ultimately control of cellular responses.

## Appendix A. Measurement of receptor upregulation and internalization at 37°C and sensitivity analysis

### A.1. Measurement of receptor upregulation at 37°C

The dependence of receptor upregulation on ligand identity and concentration was determined for three fluorescent ligands, CHO-NLFNYK-FL, CHO-MLFFK-FL, and CHO-VLFK-FL, using methods similar to those reported previously [50]. Neutrophils ( $10^6$ /ml in HSB plus  $Ca^{2+}$ ) were incubated at 37°C for 10min to allow temperature-dependent receptor upregulation to occur [21,50]. Thirty seconds before and at designated times after addition of ligand, 50  $\mu$ l aliquots were removed and diluted into 0.5ml of ice cold HSB with 29mM  $NH_4Cl_2$  to stop receptor trafficking and neutralize acidic intracellular compartments where internalized ligand fluorescence could possibly be quenched [50]. After incubation on ice for at least 10min, a saturating dose (5nM) of CHO-NLFNYK-FL was added to each sample as a 1/100 dilution of a stock in HSB plus 1mg/ml BSA. Controls to determine non-specific binding included 5nM CHO-NLFNYK-FL and a large excess of unlabeled ligand (30  $\mu$ M CHO-MLF). Binding was allowed

to equilibrate for 2 h, after which cell-associated fluorescence was measured by flow cytometry (Becton-Dickinson FACS-can). After subtraction of non-specific binding, fluorescence measurements were converted to numbers of bound receptors per cell by comparing with standardized fluorescent beads as previously described [10,13]. By subtracting the number of surface receptors at time zero from the number of receptors expressed at each time after addition of ligand, a time course of upregulated receptors was obtained.

For a single ligand concentration, receptor upregulation was modeled as depletion of receptors from an intracellular pool that was described by the equation

$$R_{\text{up}}(t) = R_{\text{pool}}(1 - e^{-k_{\text{up}}t}) \quad (\text{A1})$$

where  $R_{\text{up}}$  represents the number of receptors upregulated to the surface,  $R_{\text{pool}}$  (number per cell) is the size of the internal receptor pool before addition of ligand, and  $k_{\text{up}}$  ( $\text{s}^{-1}$ ) is the upregulation rate constant.  $R_{\text{pool}}$  was determined for the highest concentration of CHO-NLFNYK-FL (which was run for each experiment) then held constant at that value while fitting lower concentrations of CHO-NLFNYK-FL and all concentrations of other ligands. Data on upregulated receptors as a function of time were fit by least squares regression to determine  $R_{\text{pool}}$  and  $k_{\text{up}}$ . The average values and standard deviations for initial values of surface receptors and the internal pool of receptors were  $28,000 \pm 8000$  ( $n=15$ ) and  $43,000 \pm 21,000$  ( $n=21$ ) per cell, respectively. The value of the upregulation rate constant ( $k_{\text{up}}$ ) was found to be dependent upon ligand identity and concentration. Fig. A1 shows the dependence of receptor upregulation on concentration for CHO-VLFFK-FL.

For each ligand, the upregulation rate constant  $k_{\text{up}}$  was plotted as a function of ligand concentration (Fig. A2) and the data were fit with a hyperbolic function:

$$k_{\text{up}} = \frac{k_{\text{up max}}[L]}{K_m + [L]} \quad (\text{A2})$$

where  $k_{\text{up max}}$  is the maximum value of the receptor upregulation rate constant,  $L$  is the ligand concentration, and  $K_m$  is a ligand-dependent parameter equal to the concentration at which  $k_{\text{up}}$  is at half its maximal value. The ligand and concentration dependence of  $k_{\text{up}}$  then were characterized by  $K_m$  and  $k_{\text{up max}}$  values. All three ligands had similar values for  $k_{\text{up max}}$  (mean and standard deviation  $= 5.0 \pm 1.4 \times 10^{-3} \text{ s}^{-1}$ ,  $n=7$ ). With  $k_{\text{up max}}$  held at  $5.0 \times 10^{-3} \text{ s}^{-1}$ ,  $K_m$  values were estimated to be 1.2 nM, 0.11 nM, and 0.04 nM for CHO-VLFFK-FL, CHO-NLFNYK-FL, and CHO-MLFFK-FL, respectively.

For the three ligands tested,  $K_m$  values correlated with  $\text{ED}_{50}$  values for the oxidant response. These  $K_m$  values and oxidant response  $\text{ED}_{50}$  values are related by a power law function,  $K_m = A(\text{ED}_{50})^B$  where  $A$  and  $B$  are the intercept and slope of the function on a log–log plot as shown in Fig. A3. Values of the upregulation rate constant for the remaining three agonists were not easily measured directly because they are not fluorescent or else fluoresce at a wavelength that is not optimal for study using the Becton-Dickinson FACSscan. Thus values of  $K_m$  for these agonists were calculated from the data of Fig. A3 based on their

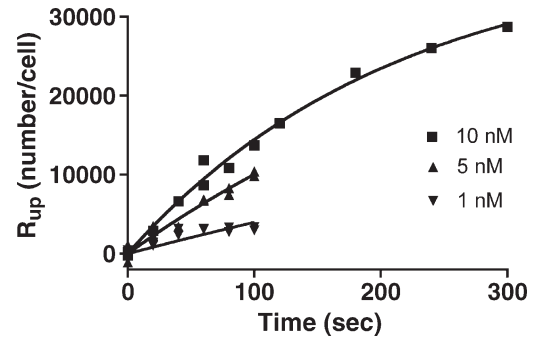


Fig. A1. Receptor upregulation rate changes with ligand concentration. For this representative experiment,  $R_{\text{pool}}(0)=38,300$  receptors per cell. Values of the upregulation rate constant  $k_{\text{up}}$  for 1 nM, 5 nM, and 10 nM CHO-VLFFK-FL were 0.0011, 0.0031, and 0.0048 ( $\text{s}^{-1}$ ), respectively.

known oxidant response  $\text{ED}_{50}$  values (listed in Fig. 1).  $K_m$  values for CHO-NLF, CHO-MLF, and CHO-NLFNYK-TMR were estimated to be 26, 6.0, and 0.41 nM, respectively. Quantitatively similar results were obtained if actin polymerization  $\text{ED}_{50}$  values were used in fitting (data not shown). Receptor upregulation is reported to be dependent on G protein activation and was therefore assumed not induced by antagonist binding [21].

Because of some uncertainty in the value of  $k_{\text{up}}$  for the three agonist not directly measured, we tested the sensitivity of our conclusions to variations in  $k_{\text{up}}$  over the entire range ( $0-0.005 \text{ s}^{-1}$ ). For example, simulations with 1 nM CHO-NLFNYK-FL predicted that  $\text{LR}_a$  levels could vary up to 2-fold as  $k_{\text{up}}$  varies, with less variation at lower ligand concentrations (data not shown). However, these variations in the number of  $\text{LR}_a$  per cell were found to be insignificant when the integral of  $\text{LR}_a$  over the initial 10 s of binding was calculated and plotted versus normalized actin polymerization and normalized oxidant production. This was due to the fact that the variation in the number of  $\text{LR}_a$  per cell was small in comparison to the 4 orders of magnitude variation in the number of  $\text{LR}_a$  due to differences in ligand potency. The resultant plots of integrated  $\text{LR}_a$  versus normalized response for simulations with and without upregulation, while quantitatively different, were qualitatively indistinguishable (data not shown). Thus our conclusions regarding the ability of Schemes 1 and 2 to fit the response data were not sensitive to these variations in  $k_{\text{up}}$ .

#### A.2. Measurement of receptor internalization at 37°C

To measure receptor internalization, neutrophils suspended at  $10^6/\text{ml}$  in HSB plus  $\text{Ca}^{2+}$  were incubated at 37°C for 10 min. Binding of CHO-MLFFK-FL and CHO-VLFFK-FL was observed by flow cytometry as described by Finney and Sklar [51]. At various times after initiating binding, 8.3  $\mu\text{l}$  of 1 mM HCl was added, dropping the extracellular pH to 3.8 and quenching the fluorescence of extracellular bound and free ligand [18,51]. Alternatively, quenching of extracellular fluorescence was achieved by adding 0.2% Trypan blue. The unquenched fluorescence represented internalized ligand–

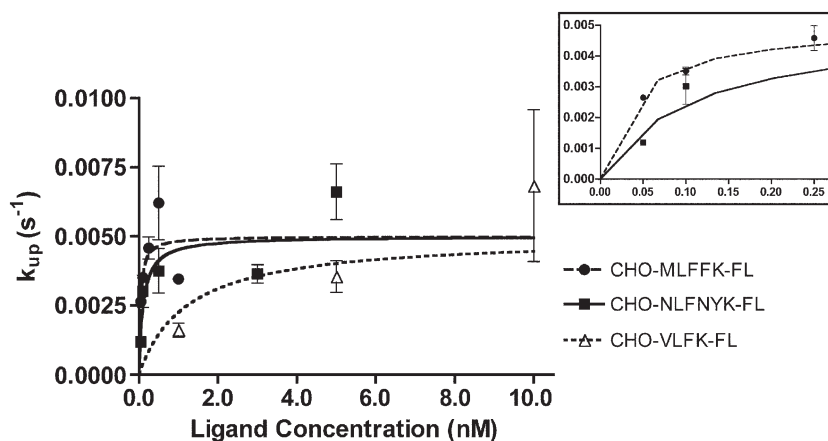


Fig. A2. Receptor upregulation rate constant  $k_{up}$  is a function of ligand concentration and ligand identity. Measured values of  $k_{up}$  for CHO-VLFK-FL, CHO-NLFNYK-FL, and CHO-MLFFK-FL are plotted as a function of ligand concentration.  $k_{up}$  for each ligand was fit by Eq. (A2) (lines). Inset:  $k_{up}$  values at low concentrations. Note that the value of  $k_{up}$  increases rapidly at low ligand concentrations.

receptor complexes at each time point and was converted to receptors/cell as previously described [10,13]. Thus a time course of internalized receptors,  $LR_{in}$ , was generated. The internalization rate constant  $k_{in}$  for CHO-MLFFK-FL and CHO-VLFK-FL were found to be  $8.8 \times 10^{-3}$  and  $11 \times 10^{-3}$  ( $s^{-1}$ ), respectively. These were comparable to the published value for CHO-NLFNYK-FL,  $3.3 \times 10^{-3}$  ( $s^{-1}$ ). Thus for the other ligands in this study  $k_{in}$  was set to  $3.3 \times 10^{-3}$  ( $s^{-1}$ ).

### A.3. Sensitivity of conclusions to difference between measured and calculated 37°C kinetic binding constants

The 37°C rate constant values and uncertainties obtained by direct measurement with data fitting or by estimation from 4°C data were similar. This suggests that neither approach has a clear advantage. However, because of some uncertainty in the values of the rate constants estimated from 4°C data, we tested the sensitivity of our conclusions to the variation in rate constant values between the measured and estimated values. For example, predicted  $LR_a$  levels over the time scale of responses (200s) could vary 3-fold between measured and estimated

values of  $k_f$  (Table 1) for a concentration of 0.1 nM CHO-MLFFK-FL (data not shown). A 20-fold difference in measured and estimated values of  $k_x$  for CHO-VLFK-FL has even less of an effect on  $LR_a$ : for 1 nM of CHO-VLFK-FL the difference in the number of  $LR_s$  per cell over the first 200s of ligand binding was approximately 2-fold (data not shown). These variations in the number of  $LR_a$  per cell were found to be insignificant when the integral of  $LR_a$  over the initial 10s of binding was calculated and plotted versus normalized actin polymerization and normalized oxidant production. As with uncertainties in the upregulation rate constant  $k_{up}$  described previously, the variation in the number of  $LR_a$  per cell was small in comparison to the 4 orders of magnitude variation in the number of  $LR_a$  due to differences in ligand potency. Thus our conclusions regarding the ability of Schemes 1 and 2 to fit the response data were not sensitive to these uncertainties in values of the kinetic binding constants.

## Appendix B. Model equations

The 37°C binding model (Scheme 1) and the modified 37°C binding model (Scheme 2) were used in this work to test for correlations between receptor species and measured responses in the *N*-formyl peptide receptor system on human neutrophils. As described in the main body of this report, both schemes allow for binding of ligand to low and high affinity surface receptors, with conversion of low to high affinity receptors occurring with rate constant  $k_x$ . At 37°C receptor upregulation from an internal receptor pool ( $R_{pool}$ ) and receptor internalization ( $LR_{in}$ ) also occur.

In Scheme 1, low affinity ligand–receptor complexes are assumed identical and termed  $LR_s$ . The equations for Scheme 1 are:

$$d[R_s]/dt = k_r[LR_s] - k_f[R_s][L] + k_{up}[R_{pool}] \quad (B1)$$

$$d[LR_s]/dt = k_f[R_s][L] - k_r[LR_s] - k_x[LR_s] \quad (B2)$$

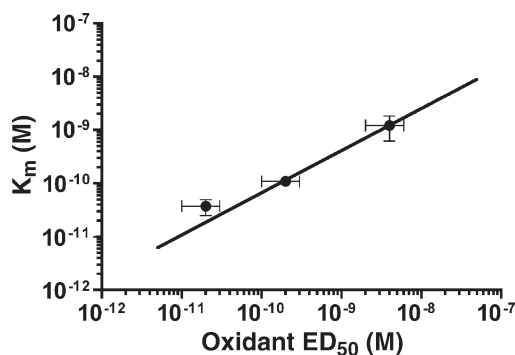


Fig. A3.  $K_m$  is correlated with the values of oxidant polymerization  $ED_{50}$ .  $K_m$  values for CHO-MLFFK-FL, CHO-NLFNYK-FL, and CHO-VLFK-FL are plotted vs. the  $ED_{50}$  concentrations of oxidant production.  $K_m$  values for CHO-NLFNYK-TMR, CHO-MLF, and CHO-NLF were estimated by a power law relationship  $K_m = A(ED_{50})^B$  where  $A=0.005$  and  $B=0.8$  are the slope and intercept, respectively.

$$d[LR_x]/dt = k_x[LR_s] + k_{r2}[R_x][L] - k_{r2}[LR_x] \quad (B3)$$

$$d[R_x]/dt = k_{r2}[LR_x] - k_{r2}[R_x][L] \quad (B4)$$

$$d[LR_{in}]/dt = k_{in}[LR_x] \quad (B5)$$

$$d[R_{pool}]/dt = -k_{up}[R_{pool}] \quad (B6)$$

In Scheme 2 low affinity ligand–receptor complexes are comprised of active ( $LR_a$ ) and inactive ( $LR_i$ ) receptor states.  $LR_a$  and  $LR_i$  are calculated from Eqs. B1, B2, B3, B4, B5, and B6 and

$$LR_s = LR_a + LR_i \quad (B7)$$

$$K_{eq} = LR_a/LR_i \quad (B8)$$

For some calculations, simultaneous binding of two ligands was simulated according to Scheme 2. To do this, Eqs. B2, B3, B5, B7, and B8 were written for each ligand with its respective rate constants. In Eqs. B1 and B4 terms were added for binding and dissociation of the second ligand, and in Eq. B6 the upregulation rate constant  $k_{up}$  was calculated using the total ligand concentration and a value for  $K_m$  that was weighted according to the individual ligand concentrations (see Appendix A for discussion of upregulation).

Simulations used the rate constants given in Table 2. Surface receptors were assumed to initially be all in the  $R_s$  state and the initial number of these surface receptors was equal to 21,000 (number/cell). The initial intracellular pool of receptors was equal to 43,000 (number/cell) and ligand was added at time equal to 0. These values of receptor total correspond to experimental averages (see Appendix A).

## References

- [1] L. Zhang, Y.K. Yu, S. Mackin, F.F. Weight, G.R. Uhl, J.B. Wang, *Journal of Biological Chemistry* 271 (19) (1996) 11449.
- [2] C. Watson, G. Chen, P. Irving, J. Way, W.-J. Chen, T. Kenakin, *Molecular Pharmacology* 58 (6) (2000) 1230.
- [3] K.A. Berg, S. Maayani, J. Goldfarb, C. Scaramellini, P. Leff, W.P. Clarke, *Molecular Pharmacology* 54 (1) (1998) 94.
- [4] D.M. Perez, S.S. Kamik, *Pharmacology Reviews* 57 (2) (2005) 147.
- [5] T. Kenakin, *Trends in Pharmacological Sciences* 16 (7) (1995) 232.
- [6] C. Gales, R.V. Rebois, M. Hogue, P. Trieu, A. Breit, T.E. Hebert, M. Bouvier, *Nature Methods* 2 (3) (2005) 177.
- [7] J.P. Nolan, L.A. Sklar, *Nature Biotechnology* 16 (7) (1998) 633.
- [8] G.M. Omann, in: M. Eisenbach (Ed.), *Chemotaxis*, Imperial College Press, 2004, p. 308.
- [9] L.A. Sklar, G.M. Omann, R.J. Painter, *Journal of Cell Biology* 101 (1985) 1161.
- [10] A. Waller, K.L. Sutton, T.L. Kinzer-Ursem, A. Absood, J.R. Traynor, J.J. Linderman, G.M. Omann, *Biochemistry* 43 (25) (2004) 8204.
- [11] L.A. Sklar, P.A. Hyslop, Z.G. Oades, G.M. Omann, A.J. Jesaitis, R.G. Painter, C.G. Cochrane, *Journal of Biological Chemistry* 260 (1985) 11461.
- [12] P.A. Hyslop, L.A. Sklar, *Analytical Biochemistry* 141 (1984) 280.
- [13] A. Waller, D. Pipkorn, K.L. Sutton, J.J. Linderman, G.M. Omann, *Cytometry* 45 (2) (2001) 102.
- [14] E.R. Prossnitz, T.L. Gilbert, S. Chiang, J.J. Campbell, S. Qin, W. Newman, L.A. Sklar, R.D. Ye, *Biochemistry* 38 (8) (1999) 2240.
- [15] S.H. Zigmond, S.J. Sullivan, D.A. Lauffenburger, *Journal of Cell Biology* 92 (1) (1982) 34.
- [16] J.F. Hoffman, M.L. Keil, T.A. Riccobene, G.M. Omann, J.J. Linderman, *Biochemistry* 35 (40) (1996) 13047.
- [17] L.A. Sklar, J. Sayre, V.M. McNeil, D.A. Finney, *Molecular Pharmacology* 28 (1985) 323.
- [18] L.A. Sklar, D.A. Finney, Z.G. Oades, A.J. Jesaitis, R.G. Painter, C.G. Cochrane, *Journal of Biological Chemistry* 259 (1984) 5661.
- [19] G.M. Omann, L.A. Sklar, *Journal of Cell Biology* 107 (3) (1988) 951.
- [20] L.A. Sklar, G.M. Bokoch, D. Button, J.E. Smolen, *Journal of Biological Chemistry* 262 (1987) 135.
- [21] J.F. Hoffman, J.J. Linderman, G.M. Omann, *Journal of Biological Chemistry* 271 (31) (1996) 18394.
- [22] L.A. Sklar, *Annual Review of Biophysics and Biophysical Chemistry* 16 (1987) 479.
- [23] L.A. Sklar, *Advances in Immunology* 39 (1986) 95.
- [24] A. Jesaitis, J. Naemura, L. Sklar, C. Cochrane, R. Painter, *Journal of Cell Biology* 98 (4) (1984) 1378.
- [25] T. Kenakin, *FASEB Journal* 15 (3) (2001) 598.
- [26] T. Kenakin, *Trends in Pharmacological Sciences* 18 (11) (1997) 416.
- [27] J.M. Weiss, P.H. Morgan, M.W. Lutz, T.P. Kenakin, *Journal of Theoretical Biology* 178 (2) (1996) 151.
- [28] P. Samama, S. Cotecchia, T. Costa, R.J. Lefkowitz, *Journal of Biological Chemistry* 268 (7) (1993) 4625.
- [29] G. Liapakis, W.C. Chan, M. Papadokostaki, J.A. Javitch, *Molecular Pharmacology* 65 (5) (2004) 1181.
- [30] P. Ghanouni, J.J. Steenhuis, D.L. Farrens, B.K. Kobilka, *Proceedings of the National Academy of Sciences of the United States of America* 98 (11) (2001) 5997.
- [31] G. Swaminath, Y. Xiang, T.W. Lee, J. Steenhuis, C. Parnot, B.K. Kobilka, *Journal of Biological Chemistry* 279 (1) (2004) 686.
- [32] M.H. Hsu, S.C. Chiang, R.D. Ye, E.R. Prossnitz, *Journal of Biological Chemistry* 272 (47) (1997) 29426.
- [33] E.R. Prossnitz, R.E. Schreiber, G.M. Bokoch, R.D. Ye, *Journal of Biological Chemistry* 270 (18) (1995) 10686.
- [34] G.M. Omann, Z.G. Oades, L.A. Sklar, *Biotechniques* 3 (1985) 508.
- [35] L.A. Sklar, H. Mueller, G.M. Omann, Z.G. Oades, *Journal of Biological Chemistry* 264 (1989) 8483.
- [36] A.J. Jesaitis, J.O. Tolley, R.A. Allen, *Journal of Biological Chemistry* 261 (29) (1986) 3662.
- [37] A.J. Jesaitis, R.W. Erickson, K.-N. Klotz, R.K. Bommakanti, D.W. Siemsen, *Journal of Immunology* 151 (1993) 5653.
- [38] D.A. Lauffenburger, J.J. Linderman, *Receptors: Models for Binding, Trafficking, and Signaling*, Oxford University Press, New York, 1993.
- [39] P.J. Munson, D. Rodbard, *Analytical Biochemistry* 107 (1980) 220.
- [40] A. Dalpiaz, A. Scatturin, G. Vertuani, R. Pecoraro, P.A. B. K. Varani, S. Traniello, S. Spisani, *European Journal of Pharmacology* 411 (3) (2001) 327.
- [41] T. Kenakin, *Trends in Pharmacological Sciences* 24 (7) (2003) 346.
- [42] S.H. Zigmond, *Current Opinion in Cell Biology* 8 (1) (1996) 66.
- [43] H. Mueller, R. Weingarten, L.A. Ransnas, G.M. Bokoch, L.A. Sklar, *Journal of Biological Chemistry* 266 (20) (1991) 12939.
- [44] L.A. Sklar, G.M. Omann, *Seminars in Cell and Developmental Biology* 1 (2) (1990) 115.
- [45] R.J. Lefkowitz, S. Cotecchia, P. Samama, T. Costa, *Trends in Pharmacological Sciences* 14 (8) (1993) 303.
- [46] P. Leff, C. Scaramellini, C. Law, K. McKechnie, *Trends in Pharmacological Sciences* 18 (10) (1997) 355.
- [47] C. Scaramellini, P. Leff, *Annals of the New York Academy of Sciences* 861 (1998) 97.
- [48] U. Gether, S. Lin, B. Kobilka, *Journal of Biological Chemistry* 270 (1995) 28268 (Nov. 24).

- [49] T. Palanche, B. Ilien, S. Zoffmann, M.-P. Reck, B. Bucher, S.J. Edelstein, J.-L. Galzi, *Journal of Biological Chemistry* 276 (37) (2001) 34853.
- [50] J. Norgauer, M. Eberle, S.P. Fay, H.D. Lemke, L.A. Sklar, *Journal of Immunology* 146 (3) (1991) 975.
- [51] D.A. Finney, L.A. Sklar, *Cytometry* 4 (1983) 54.
- [52] R.D. Ye, F. Boulay, *Advances in Pharmacology* 39 (1997) 221.
- [53] S. Fiore, S.W. Ryeom, P.F. Weller, C.N. Serhan, *Journal of Biological Chemistry* 267 (23) (1992) 16168.
- [54] O. Quehenberger, E.R. Prossnitz, S.L. Cavanagh, C.G. Cochrane, R.D. Ye, *Journal of Biological Chemistry* 268 (24) (1993) 18167.